J|A|C|S

A R T I C L E S

Solution-Phase Single Quantum Dot Fluorescence Resonance Energy Transfer

Thomas Pons,[†,∥] Igor L. Medintz,[‡] Xiang Wang,[§] Douglas S. English,[§] and Hedi Mattoussi*,[†]

Contribution from the Optical Sciences Division, Code 5611, Center for Bio/Molecular Science and Engineering, Code 6900, Naval Research Laboratory, Washington, D.C. 20375, and Department of Chemistry and Biochemistry, University of Maryland, College Park, Maryland 20742

Received August 7, 2006; E-mail: hedi.mattoussi@nrl.navy.mil

Abstract: We present a single particle fluorescence resonance energy transfer (spFRET) study of freely diffusing self-assembled quantum dot (QD) bioconjugate sensors, composed of CdSe−ZnS core−shell QD donors surrounded by dye-labeled protein acceptors. We first show that there is direct correlation between single particle and ensemble FRET measurements in terms of derived FRET efficiencies and donor−acceptor separation distances. We also find that, in addition to increased sensitivity, spFRET provides information about FRET efficiency distributions which can be used to resolve distinct sensor subpopulations. We use this capacity to gain information about the distribution in the valence of self-assembled QD−protein conjugates and show that this distribution follows Poisson statistics. We then apply spFRET to characterize heterogeneity in single sensor interactions with the substrate/target and show that such heterogeneity varies with the target concentration. The binding constant derived from spFRET is consistent with ensemble measurements.

Introduction

Single molecule measurements have brought a wealth of information and allowed better understanding of a wide range of physical, chemical, and biological phenomena and processes.[1,2] For example, single molecule detection is able to resolve molecular scale heterogeneities in macroscopically homogeneous samples (e.g., a dispersion of nanoparticles), compared to ensemble measurements. In particular, ratiometric detection of single Fluorescence Resonance Energy Transfer (FRET) pairs provides information about donor−acceptor distance distributions, receptor−ligand binding, and macromolecule conformation.[3,4] Two experimental modalities may be used to achieve single molecule detection. Immobilization of molecules on substrates affords the ability to resolve time-dependent changes of isolated molecules and characterize the dynamics of interconversion between substates (e.g., protein folding conformations), without having to synchronize a large population. Alternatively, detection of freely diffusing single molecules

with a confocal microscope setup allows rapid monitoring of large populations and is not subject to surface-induced artifacts.

Luminescent semiconductor nanocrystals, or quantum dots (QDs), offer several advantages as fluorophores over traditional organic dyes for biological sensing and imaging.[5−12] These include broad excitation spectra, large one- and two-photon absorption cross sections, and narrow size-tunable photoluminescence (PL) emission spectra along with excellent photostability and chemical stability. Thanks to recent advances in QD solubilization and bioconjugation techniques, these probes are being increasingly used in a wide variety of in vitro and in vivo applications, ranging from immunoassays to cellular labeling and tissue imaging.[13−18]

[†] Optical Sciences Division, Naval Research Laboratory.
[‡] Center for Bio/Molecular Science and Engineering, Naval Research Laboratory.
[§] University of Maryland.
[∥] Also at Chemical and Biomolecular Engineering Department, Johns Hopkins University, Baltimore, MD 21218.

(1) Deniz, A. A.; Laurence, T. A.; Dahan, M.; Chemla, D. S.; Schultz, P. G.; Weiss, S. *Annu. Rev. Phys. Chem.* **2001**, *52*, 233−253.
(2) Xie, X. S.; Trautman, J. K. *Annu. Rev. Phys. Chem.* **1998**, *49*, 441−480.
(3) Deniz, A. A.; Dahan, M.; Grunwell, J. R.; Ha, T.; Faulhaber, A. E.; Chemla, D. S.; Weiss, S.; Schultz, P. G. *Proc. Natl. Acad. Sci. U.S.A.* **1999**, *96*, 3670−3675.
(4) Ha, T.; Ting, A. Y.; Liang, J.; Caldwell, W. B.; Deniz, A. A.; Chemla, D. S.; Schultz, P. G.; Weiss, S. *Proc. Natl. Acad. Sci. U.S.A.* **1999**, *96*, 893−898.
(5) Murray, C. B.; Norris, D. J.; Bawendi, M. G. *J. Am. Chem. Soc.* **1993**, *115*, 8706−8715.
(6) Hines, M. A.; Guyot-Sionnest, P. *J. Phys. Chem.* **1996**, *100*, 468−471.
(7) Dabbousi, B. O.; RodriguezViejo, J.; Mikulec, F. V.; Heine, J. R.; Mattoussi, H.; Ober, R.; Jensen, K. F.; Bawendi, M. G. *J. Phys. Chem. B* **1997**, *101*, 9463−9475.
(8) Bruchez, M.; Moronne, M.; Gin, P.; Weiss, S.; Alivisatos, A. P. *Science* **1998**, *281*, 2013−2016.
(9) Chan, W. C. W.; Nie, S. M. *Science* **1998**, *281*, 2016−2018.
(10) Alivisatos, P. *Nat. Biotechnol.* **2004**, *22*, 47−52.
(11) Medintz, I. L.; Uyeda, H. T.; Goldman, E. R.; Mattoussi, H. *Nat. Mater.* **2005**, *4*, 435−446.
(12) Michalet, X.; Pinaud, F. F.; Bentolila, L. A.; Tsay, J. M.; Doose, S.; Li, J. J.; Sundaresan, G.; Wu, A. M.; Gambhir, S. S.; Weiss, S. *Science* **2005**, *307*, 538−544.
(13) Wu, X.; Liu, H.; Liu, J.; Haley, K. N.; Treadway, J. A.; Larson, J. P.; Ge, N.; Peale, F.; Bruchez, M. P. *Nat. Biotechnol.* **2003**, *21*, 41−46.
(14) Goldman, E. R.; Clapp, A. R.; Anderson, G. P.; Uyeda, H. T.; Mauro, J. M.; Medintz, I. L.; Mattoussi, H. *Anal. Chem.* **2004**, *76*, 684−688.
(15) Jaiswal, J. K.; Mattoussi, H.; Mauro, J. M.; Simon, S. M. *Nat. Biotechnol.* **2003**, *21*, 47−51.
(16) Dubertret, B.; Skourides, P.; Norris, D. J.; Noireaux, V.; Brivanlou, A. H.; Libchaber, A. *Science* **2002**, *298*, 1759−1762.

The QDs' unique spectroscopic properties also make them particularly suitable as FRET donors.[19−22] In particular, their broad absorption spectra allow excitation of the QDs far from the acceptor absorption spectrum which limits acceptor direct excitation, while their narrow emissions allow easy signal separation and simplify data analysis. This has led to the development of several QD-based FRET assays for DNA and small analyte detection.[20,22−24] A recent report by Wang et al. used commercially available Streptavidin-coated QDs to demonstrate single particle sensing of DNA hybridization based on QD and FRET.[24] The authors used the strong reduction of acceptor direct excitation to improve assay sensitivity compared to studies that used organic dye molecular beacons. However, the long separation distances in their QD−streptavidin−biotin−oligomer−acceptor construct limited the energy transfer efficiency from one QD to one acceptor to about 4%. While more efficient energy transfer may be achieved by conjugating a high number of acceptors per QD, signals from a single QD−protein conjugate then represents an average signal from all the protein−dyes conjugated to the particle, which undermines the interest of single particle detection. In this regard, higher donor-to-single acceptor FRET efficiencies would result in higher sensitivities and give access to more quantitative information about heterogeneous sensor populations.

Here, we report a full FRET characterization of solution-phase single dye-labeled protein−QD bioconjugates, with efficient donor-to-single acceptor energy transfer. We first show the quantitative equivalence between single particle FRET (spFRET) and ensemble measurements in terms of derived averaged FRET efficiencies and donor−acceptor distances. We then use single particle FRET to resolve heterogeneity in individual self-assembled bioconjugates within a population and test these findings in two applications. First, we resolve the distribution in the number of protein acceptor per QD in a solution of QD−protein conjugates (macroscopic sample) with a given nominal protein-to-QD ratio. In particular, we show that the valence of self-assembled QD−protein conjugates follows a Poisson statistics. We then demonstrate single particle sensing/binding of a conjugated protein to its substrate analyte and identify two sensor subpopulations, one representing "free" sensors (QD conjugates not interacting with the analyte) and the other made of sensors that are bound to the target molecule.

Materials and Methods

Quantum Dots. Semiconductor CdSe−ZnS core−shell nanocrystal QDs were synthesized using organometallic precursors injected at high temperature, following published procedures.[5−7,25] Two QD samples were prepared exhibiting narrow and symmetric emission spectra

centered at 520 and 540 nm, respectively. The QDs were transferred to an aqueous buffer by exchanging the native trioctylphosphine/trioctylphosphine oxide (TOP/TOPO) ligands with dihydrolipoic acid (DHLA).[26] The resulting QDs were stable and aggregate-free in basic buffer for several months, as verified by dynamic light scattering.[27]

QD−Protein Conjugation. The *E. coli* derived maltose binding protein (MBP) was modified with a C-terminal pentahistidine sequence using procedures described elsewhere.[20,28] These proteins were engineered to express a unique cysteine amino acid at either position 95 (MBP95C) or position 41 (MBP41C). This allowed for site-specific labeling of the proteins with Rhodamine Red (RR)-, Cy3-, or Cy5-maleimide dyes. The affinity of the polyhistidine tract to ZnS overcoated CdSe nanocrystals allowed easy and stable self-assembly of the proteins on the QDs' surface. The QD−MBP conjugates were prepared by mixing DHLA-capped QDs, unlabeled MBP, and dye-labeled MBP in ratiometric quantities in 10 mM Na-tetraborate buffer (pH ≈ 9). Conjugation of proteins is accompanied with a QD ensemble quantum yield (QY) increase in solution, which has been attributed to better surface passivation and neutralization of electric field effects at the surface of DHLA-capped QDs.[20,26] To minimize sample-to-sample QY variations, the total number of proteins was kept constant while varying the ratio of unlabeled-to-labeled proteins per QD bioconjugate.

QD−Dye Labeled Protein FRET. Self-assembly of dye-labeled proteins onto the QDs brings the dye acceptors in close proximity to the QD center and results in efficient FRET.[20,21] The site-specific protein labeling and controlled orientation of the protein on the QD afforded by the metal-affinity-driven conjugation provide homogeneous donor−acceptor separation distances within these conjugates (Figure 1A).[21,29] The energy transfer efficiency from a QD conjugated to exactly n acceptors at a distance r from the QD center is given by [21,30]

$$E(n) = \frac{nR_0^6}{nR_0^6 + r^6} \tag{1}$$

where R_0 is the Förster radius (distance at which the efficiency for a donor−single acceptor pair becomes 0.5). Absorption and emission spectra of the different QD/dye pairs are provided in the Supporting Information, Figure S3.

For each sample, ensemble PL emission spectra were collected using a SPEX Fluorolog-3 fluorimeter and an excitation wavelength of 488 nm from a Xe lamp.

Single Particle FRET Measurements. Single particle FRET measurements were performed on an Axiovert 200 (Carl Zeiss) confocal microscope setup, previously described in ref 31 (Figure 1B). 100 μL of QD samples (3 nM in borate buffer) were placed on top of a glass coverslip above the objective. A 488 nm excitation from an argon ion laser was focused ∼10 μm above the glass surface through a 100× objective (Fluar, NA = 1.3, Carl Zeiss). The excitation intensity typically corresponded to 20−40 μW at the objective rear aperture. Fluorescence signals were collected through the same objective using a 515DCLP dichroic mirror (Chroma, Rockingham, VT; Dichroic 1 in Figure 1B), which removes contribution from the laser signal. Residual excitation light was filtered out using a 488 nm notch filter (Kaiser Optical Systems, Ann Arbor, MI). Donor and acceptor signals were separated using a 585DCXR dichroic filter (Chroma; Dichroic 2 in

(17) Dahan, M.; Levi, S.; Luccardini, C.; Rostaing, P.; Riveau, B.; Triller, A. *Science* **2003**, *302*, 442−445.
(18) Kim, S.; Lim, Y. T.; Soltesz, E. G.; De Grand, A. M.; Lee, J.; Nakayama, A.; Parker, J. A.; Mihaljevic, T.; Laurence, R. G.; Dor, D. M.; Cohn, L. H.; Bawendi, M. G.; Frangioni, J. V. *Nat. Biotechnol.* **2004**, *22*, 93−97.
(19) Patolsky, F.; Gill, R.; Weizmann, Y.; Mokari, T.; Banin, U.; Willner, I. *J. Am. Chem. Soc.* **2003**, *125*, 13918−13919.
(20) Medintz, I. L.; Clapp, A. R.; Mattoussi, H.; Goldman, E. R.; Fisher, B.; Mauro, J. M. *Nat. Mater.* **2003**, *2*, 630−638.
(21) Clapp, A. R.; Medintz, I. L.; Mauro, J. M.; Fisher, B. R.; Bawendi, M. G.; Mattoussi, H. *J. Am. Chem. Soc.* **2004**, *126*, 301−310.
(22) Gill, R.; Willner, I.; Shweky, I.; Banin, U. *J. Phys. Chem. B* **2005**, *109*, 23715−23719.
(23) Levy, M.; Cater, S. F.; Ellington, A. D. *ChemBioChem* **2005**, *6*, 2163−2166.
(24) Zhang, C.; Yeh, H.; Kuroki, M. T.; Wang, T. *Nat. Mater.* **2005**, *4*, 826−831.
(25) Peng, Z. A.; Peng, X. G. *J. Am. Chem. Soc.* **2001**, *123*, 183−184.
(26) Mattoussi, H.; Mauro, J. M.; Goldman, E. R.; Anderson, G. P.; Sundar, V. C.; Mikulec, F. V.; Bawendi, M. G. *J. Am. Chem. Soc.* **2000**, *122*, 12142−12150.
(27) Pons, T.; Uyeda, H. T.; Medintz, I. L.; Mattoussi, H. *J. Phys. Chem. B* **2006**, *110*, 20308−20316.
(28) Medintz, I. L.; Goldman, E. R.; Lassman, M. E.; Mauro, J. M. *Bioconjugate Chem.* **2003**, *14*, 909−918.
(29) Medintz, I. L.; Konnert, J. H.; Clapp, A. R.; Stanish, I.; Twigg, M. E.; Mattoussi, H.; Mauro, J. M.; Deschamps, J. R. *Proc. Natl. Acad. Sci. U.S.A.* **2004**, *101*, 9612−9617.
(30) Förster, T. *Annalen Der Physik* **1948**, *2*, 55−75.
(31) Morgan, M. A.; Okamoto, K.; Kahn, J. D.; English, D. S. *Biophys. J.* **2005**, *89*, 2588−2596.
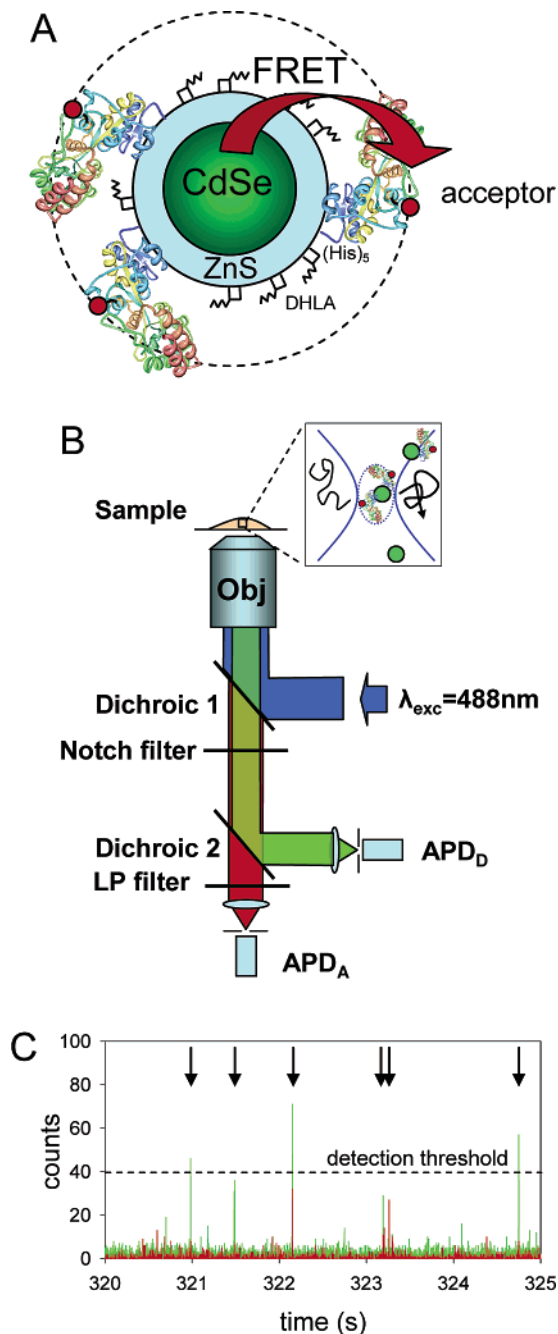
Figure 1. (A) Schematics representing a DHLA-capped semiconductor QD donor conjugated to several dye acceptor-labeled proteins. (B) spFRET detection setup. (C) Example of superimposed QD donor (green) and acceptor (red) time traces. Only the fluorescence bursts with the sum of both signals above the threshold level (indicated by arrows) are selected for analysis.

Figure 1B) for the 540 nm QD−RR and 540 nm QD−Cy5 pairs. Alternatively, a 565DCLP dichroic (Chroma) was used for the 520 nm QD−Cy3 pair in combination with a 500 nm long pass filter (Andover Corp., Salem, NH) inserted in the dye channel to remove the contribution from the dichroic transmission window below 500 nm. In both cases, the second dichroic filter was selected with a cutoff wavelength far removed from the QD emission to completely eliminate any "bleed-through" into the dye channel, a choice that corrects for heterogeneity in the spectral emission of individual QDs within a single population.[32] If the dichroic cutoff region had a significant spectral

(32) Empedocles, S. A.; Norris, D. J.; Bawendi, M. G. *Phys. Rev. Lett.* **1996**, 77, 3873−3876.

overlap with the QD ensemble emission spectrum, individual QDs would present different transmissions into the dye channel, which prevents homogeneous QD bleed-through correction. Organic dye molecules exhibit more homogeneous spectra, and their bleed-through into the QD channel is therefore easier to account for and correct. Fluorescence signals of the QD donors and dye acceptors were detected by two single-photon counting avalanche photodiodes (APD) (Perkin-Elmer, Fremont, CA). The corresponding time traces were recorded for 10 min, with 1 ms time bins, using a PCI 6602 acquisition board (National Instruments, Austin, TX) and a custom software written in Labview (National Instruments). The time traces consisted of a series of signal bursts corresponding to the diffusion of a single QD conjugate in the confocal volume, separated by periods of blank signals (Figure 1C). This shows that on average much less than one QD conjugate was present in the confocal volume during the acquisition interval (bin), due to the low sample concentration; this guarantees that the probability of detecting several conjugates simultaneously is negligible.

Single Particle FRET Analysis. Analysis of the spFRET data was performed using custom routines in Igor Pro (Wavemetrics, Lake Oswego, OR).[31] After subtraction of the background level, the dye bleed-through into the QD channel was corrected using ensemble emission spectra and the dichroic transmission responses. To provide a sufficient signal-to-noise ratio, signal bursts were selected when the sum of the two signals reached a threshold of typically 40 counts/ms (the background level was typically 4 counts/ms). The total number of such signal bursts in a single acquisition was generally ≥ 1000. In the absence of acceptor direct excitation, the FRET efficiency E of a single donor−acceptor pair is given by $E = I_A/(I_A + (\Phi_A/\Phi_D)I_D)$, where I_A (I_D) and Φ_A (Φ_D) represent the acceptor (donor) signals and quantum yields, respectively. In the present study we however opt to characterize each burst using the emission ratio $\eta = I_A/(I_A + I_D)$. When the donor is conjugated to n acceptors, η is given by

$$\eta = \frac{E(n) + n\sigma_A/\sigma_D}{(\Phi_D/\Phi_A)(1 - E(n)) + E(n) + n\sigma_A/\sigma_D} \quad (2)$$

where $E(n)$ is given by eq 1 and we take into account the possibility of acceptor direct excitation by introducing σ_A (σ_D), the acceptor (donor) excitation cross-sections at the laser wavelength. Population distributions were then characterized by their histograms evaluating the fraction of signal bursts (QD conjugates) exhibiting specific emission ratios.[1] Donor quenching efficiencies were also determined by measuring the average QD PL intensities from the population of bursts exhibiting ($I_A + I_D$) larger than the detection threshold. Here, the acceptor reemission compensates well for the donor quenching, which prevents the detection threshold from truncating the QD donor population, by allowing the detection of the efficiently quenched QDs.

Results and Discussion

1. Comparison between Single Particle and Ensemble FRET Measurements. We begin by demonstrating the equivalence between QD-based single particle FRET and ensemble FRET measurements. Figure 2A shows the ensemble emission spectra of 540 nm QD−MBP95C−RR conjugates with different ratios of RR-labeled proteins per QD−conjugate. The total number of proteins was kept constant at 12 using a mixture of labeled and unlabeled MBPs. Data clearly show that conjugation of the MBP95C−RR brings the RR dye in close proximity to the QD and results in efficient FRET, with a transfer efficiency that systematically increases with increasing number of protein acceptors around a QD donor. This is reflected by the progressive quenching of the QD PL with a concomitant increase in the RR acceptor signal as the dye-to-QD ratio increases.[21]
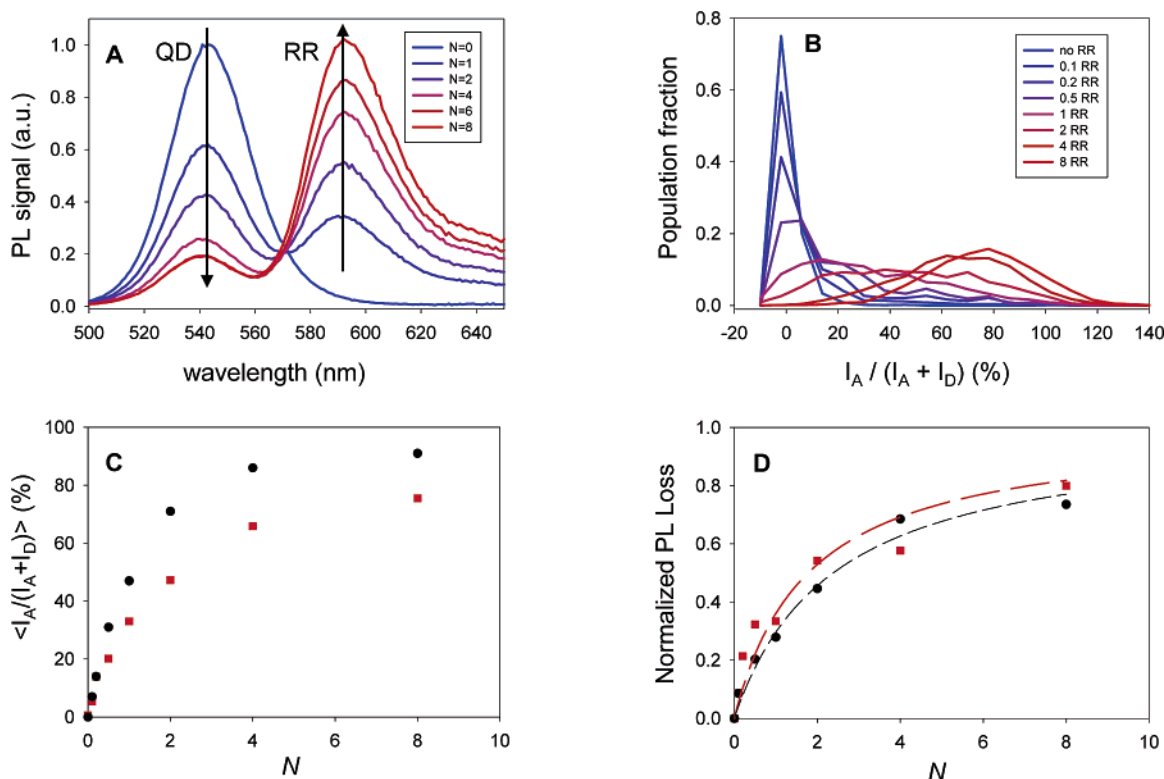
Figure 2. 540 nm QDs conjugated with a different average number N of RR-labeled proteins per QD. (A) Normalized ensemble PL spectra; (B) Emission ratio distributions obtained from spFRET measurements. (C) Comparison between ensemble (from (A); ●) and average spFRET (distribution first moments from (B); ■) emission ratios, as a function of the average number of RR acceptors per QD. (D) Normalized QD PL loss obtained from ensemble (●) and spFRET measurements (■), as a function of the average number of RR acceptors per QD.

Figure 2B shows the population distribution of the emission ratio $\eta = I_A/(I_A + I_D)$. Unphysical values below 0 and above 100% arise from noise in the background subtraction and dye bleed-through correction. The QD−MBP conjugate sample (without any acceptors) provides a relatively narrow and sharp peak centered at $\eta = 0$; this implies that the signal from all single QDs is mainly detected in the blue region of the dichroic emission. As the ratio of labeled proteins per QD increases, the peak at $\eta = 0$ diminishes and the population distribution progressively shifts toward higher emission ratios, corresponding to higher FRET efficiencies. We note the absence of bursts exhibiting $\eta \approx 100\%$ for low acceptor-to-QD ratios, which would correspond to acceptor-only emissions. Similarly, no fluorescence bursts were detected from a protein−acceptor-only solution. This indicates that acceptor emission due to direct excitation is below the detection threshold and further proves that any contribution to the acceptor channel must result from FRET within QD−protein−dye conjugates; at higher ratios additional contribution due to simultaneous (and cumulative) direct excitation of multiple acceptors conjugated to the same QD become nonnegligible (eq 2). We also observed no decrease in the density or intensity of fluorescent bursts during the course of 10 min measurements, which reflects the absence of any significant QD or dye photobleaching.

Figure 2C shows the average emission ratios η as a function of the number of labeled proteins per QD, for ensemble PL data (shown in Figure 2A) and spFRET data (shown in Figure 2B) using the distribution first moment for the spFRET data. The spFRET data exhibit slightly smaller values than their ensemble counterparts, which may be attributed to a combination of a slightly underestimated RR acceptor bleed-through into the

QD channel, different detector spectral responses, or a different behavior of the acceptor undergoing higher excitation rates in the spFRET measurements (due for example to the influence of dye triplet states). Regardless, ensemble and spFRET values follow a similar behavior and are consistent with the expected trend for energy transfer efficiencies with an increasing number of acceptors per donor.[21] FRET efficiencies derived using donor quenching often yield more reliable estimates than those derived using acceptor emission, because they do not depend on the acceptor fluorophores QY.[33] As shown in Figure 2D, when analysis was limited to QD PL loss, the two techniques yielded very similar efficiencies. Fitting these data with the expected behavior for a Förster formalism, $\Delta PL(N)/PL_0 \approx E(N) = N/(N + (r/R_0)^6)$, yields a donor−acceptor separation distance of ∼70 ± 3 Å for ensemble and 67 ± 3 Å for spFRET measurements ($R_0 \approx 60$ Å for this pair). Ensemble and spFRET measurements thus provide consistent information about average emission ratios, FRET efficiencies, and donor−acceptor separation distances. This confirms the suitability of spFRET measurements for QD-based FRET assays.

2. Distribution in the QD−Protein−Dye Conjugate Valence. Self-assembly of QD−protein bioconjugates is a process that inherently leads to a heterogeneous distribution in the number of proteins per conjugate, like any conjugation approach where multiple copies of a target receptor can interact with the QD surface functionalities. Knowledge of this distribution is of crucial importance to the design and characterization of QD-based biosensors. The number of protein acceptors per conjugate is expected to follow Poisson statistics for protein-to-QD ratio

(33) Lakowicz, J. R. *Principles of Fluorescence Spectroscopy*, 2nd ed.; Kluwer Academic: New York, 1999.
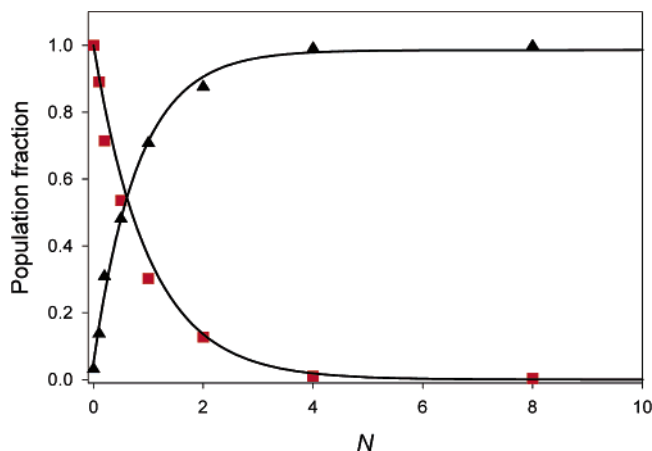
Figure 3. Fraction of QDs without any acceptors ($\eta < 10\%$; ■) and engaged in FRET ($\eta > 15\%$; ▲) as a function of N, the average number of RR acceptors per QD, obtained from spFRET measurements. The fit corresponds to the Poisson distribution $p(N,0) = \exp(-N)$.

below the QD surface saturation level (here $\sim15-20$ MBP per QD). For a conjugate with a nominal valence N (N being the average acceptor-to-QD ratio used during reagent mixing), the fraction of QDs conjugated to exactly n acceptors is then theoretically given by

$$p(N,n) = N^n \exp(-N)/n! \qquad (3)$$

We use spFRET to gain information about heterogeneity in a single QD bioconjugate valence, probe the distribution in the number of protein−dyes per QD, and compare it to the predictions of eq 3. Figure 2B reveals broad distributions of emission ratios, or FRET efficiencies, especially at an average number of protein acceptors per QD donor $N > 1$. Indeed, these distributions reflect the heterogeneity in the QD−protein−dye conjugate valence.

We first consider the fraction of QDs that are not conjugated to any acceptors, $p(N,n = 0)$. Equation 3 indicates that this fraction is expected to decrease exponentially with N:

$$p(N,0) = \exp(-N) \qquad (4)$$

Experimentally, we identify the fraction of conjugate population exhibiting an emission ratio $\eta \leq 10\%$ as QDs that are not conjugated to any protein acceptor. Figure 3 shows that this fraction follows closely the trend anticipated from eq 4. Consistently, the QD fraction exhibiting emission ratios greater than 15%, representing the QDs engaged in FRET, progressively increases with the average ratio of acceptors per QD, as $1 - p(N,n = 0)$.

We examine if the experimentally observed distributions correspond to the expected Poisson statistics for each average number of acceptors N per QD conjugate. We use eqs 1 and 2 along with donor−acceptor separation distances, acceptor direct excitation, and quantum yield ratios derived from experimental ensemble measurements to predict the emission ratios expected for a QD conjugated to exactly n acceptors. We assume that the subpopulation distributions have a Gaussian shape and attribute a common distribution width to all subpopulations to account for experimental noise and small conjugate heterogeneities. We use eq 3 to predict the relative proportion of each population component. We finally construct the theoretical population distribution, P(η), as the sum of all these subpopu-
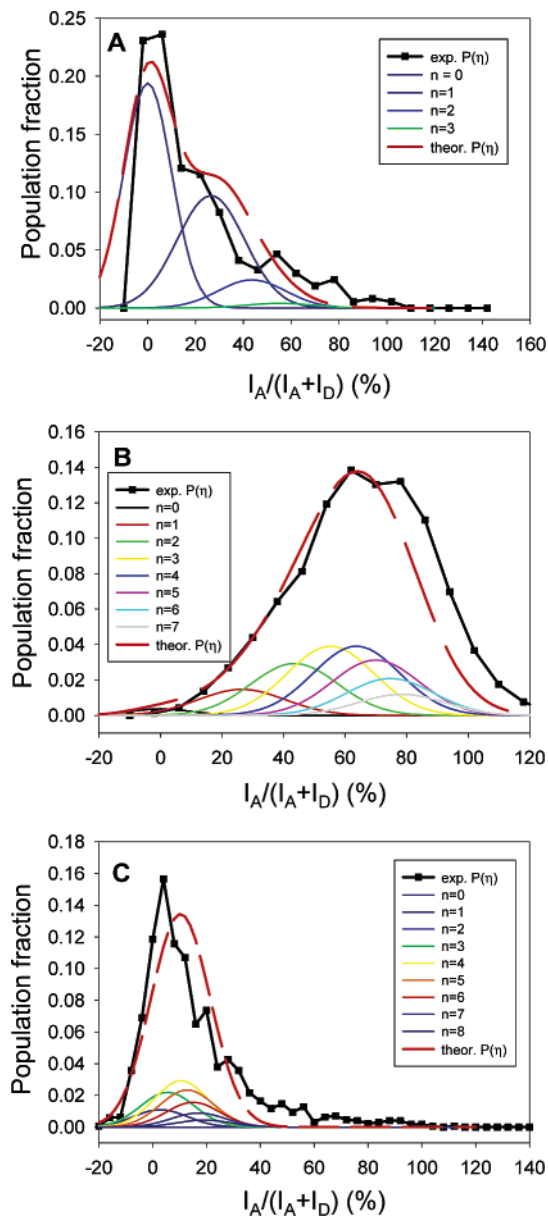
Figure 4. Experimental emission ratio distributions compared with fits from the Poisson distribution: 540 nm QDs conjugated with (A) $N = 0.5$ MBP95C−RR per QD; (B) $N = 4$ MBP95C−RR per QD; (C) $N = 4$ MBP95C−Cy5 per QD. The contributions from the different subpopulations ($n = 0, 1, 2...$) are plotted for each value N, along with their sum, P(η), and compared with the experimental curve.

lations ($n = 0, 1, 2 ...$) and compare it to the experimentally observed distribution in ratios η. Figure 4A and 4B show both experimental and theoretical distributions for $N = 0.5$ and $N = 4$ (corresponding figures for the other values of N are available in the Supporting Information, Figure S2). These distributions match throughout the range of N values used in this study, with the only fitting parameter being the subpopulations width. The slight difference between the experimental distribution and the theoretical fit at large η may be due to a poor estimation of the acceptor spectral cross-talk and/or direct excitation, or QD blinking.

To explore effects of variation in the degree of spectral overlap we compared the distribution of FRET ratios for this relatively "good" FRET pair (high spectral overlap) with that of 540 nm QD−Cy5 pair (shown in Figure 4C); the poor overlap

between 540 nm QDs and Cy5 (absorption shoulder at ∼610 nm) results in a very low FRET efficiency ($R_0 \approx 42$ Å, $E(n = 1) \approx 4\%$). Data show that this FRET pair yields a narrower distribution of emission ratios, and the different subpopulations cannot be resolved as efficiently, a direct consequence of this weaker spectral overlap (compare Figure 4B and 4C).

3. Single Particle Sensing of Small Analytes. We now examine the potential of our self-assembled QD−MBP−dye conjugates as substrates for FRET-based small analyte sensing at the single particle level. Here, the residue cysteine 41C used for attachment of a Cy3 (acceptor) is located at a position such that the obligatory conformational change in the MBP upon binding to maltose (its substrate) alters the environment around the dye and causes a drop in its quantum yield (reagentless sensor for maltose).[34] Binding of maltose does not affect the FRET efficiency, because the protein conformational change does not modify the donor−acceptor separation distance or spectral overlap. However, the drop in the Cy3 emission provides a clear optical signature of the presence of maltose (Figure S3). Here, the QD plays the dual role of an energy donor and a reference signal.

Figure 5A shows the change in the ensemble emission spectra of QD−MBP41C−Cy3 conjugates in response to increases in maltose concentration. As expected increasing maltose concentration causes the Cy3 signal to progressively decrease while the QD signal remains constant. Plotting the relative Cy3 fluorescence drop ($\Delta PL(Cy3)/\Delta PL_{max}(Cy3)$) against the maltose concentration, shown in Figure 5C, yields an apparent binding constant $K_d \approx 0.8$ mM, consistent with previously derived values.[34] Figure 5B shows the corresponding data derived from spFRET measurements. In the absence of maltose, most QD bioconjugates exhibit high emission ratios. When maltose is added to the solution, the fraction of sensors with a high emission ratio decreases while that of low emission ratio sensors progressively increases. This picture is consistent with the one assembled for ensemble measurements, as reduced Cy3 emission produces a shift toward lower emission ratios. We assessed the spFRET response of the sensing assemblies by measuring the fraction of QD conjugate sensors exhibiting low emission ratios ($\eta < 20\%$, where most of the gain occurs). Again, the spFRET response is consistent with the ensemble measurements, as shown in Figure 5C. The spFRET detection yields a binding constant $K_d \approx 2$ mM, a value close to the one extracted from macroscopic measurements.[34]

Compared to ensemble measurements which only offer average values, spFRET measurements also allowed us to gain additional insights into the heterogeneity of population distributions. In particular, ensemble measurements cannot distinguish between two distinct scenarios: (1) a homogeneous and progressive drop in Cy3 PL QY of all QD−MBP sensors in the sample or (2) the mixing of two distinct populations with high and low Cy3 photoemissions, respectively. In contrast, spFRET results reflect the coexistence of two sensor populations, one bound to (interacting with) maltose and another made of free conjugates (not bound to maltose). Furthermore, the emission ratio distribution for any intermediate maltose concentration can be described by a mix of free and bound populations, where the fraction of bound sensors progressively

(34) Medintz, I. L.; Clapp, A. R.; Melinger, J. S.; Deschamps, J. R.; Mattoussi, H. *Adv. Mater.* **2005**, *17*, 2450−2455.
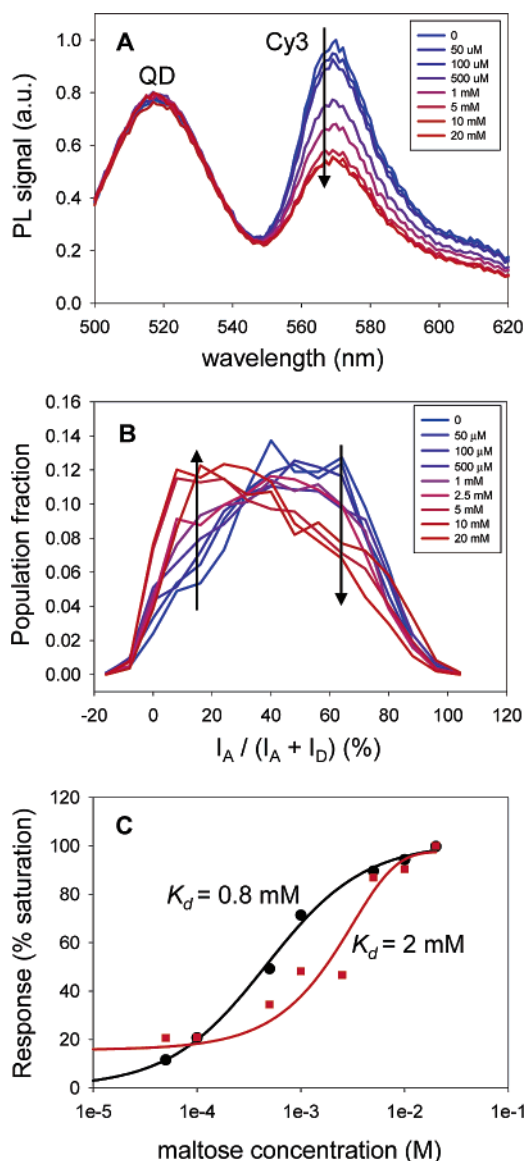

Figure 5. Maltose sensing: (A) Ensemble PL spectra of the 520 nm QD−MBP41C−Cy3 sensor and (B) spFRET emission ratio distributions, as a function of maltose concentration. (C) Response of the sensor from ensemble PL (black, ●) and spFRET measurements (red, ■).

increases with the maltose concentration. To illustrate this, we consider the population distribution in the presence of maltose at a concentration close to K_d. At this concentration, about half of the sensors should be bound to maltose. Indeed, Figure 6A shows that the conjugate population is very well fitted using a mixture of free and bound QD−MBP41C−Cy3 conjugates. The distributions of free and bound sensors were collected from the samples in the absence of maltose and under saturation conditions (with 20 mM maltose), respectively, with free sensor distribution being mainly weighted toward higher η and that of bound sensors weighted toward the lower η values. In contrast, the other possible scenario (characterized by a progressive homogeneous quenching of Cy3 fluorescence in the presence of maltose) would lead to a shift in the initial emission ratio distribution (in absence of maltose) toward lower values (as shown in Figure 6B). The predicted shifted distribution for the same maltose concentration considered above is very different from the measured one. The spFRET measurements thus unambiguously reveal the coexistence of two distinct sensor
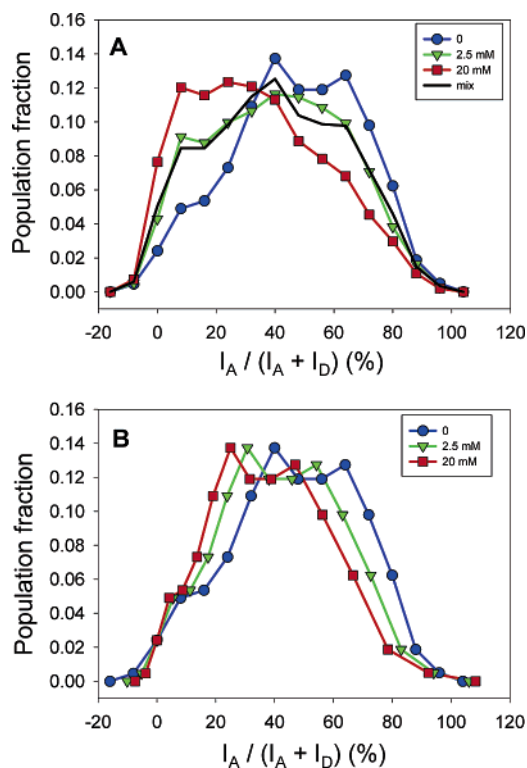
Figure 6. (A) Distribution of emission ratios derived from spFRET experiments. The population derived for 2.5 mM of added maltose (green) is well described using a mixture (black) of two populations, one in absence of maltose (blue) and one under saturation conditions with 20 mM maltose (red). (B) For comparison, the corresponding "theoretical" population distributions are shown, assuming homogeneous progressive response of all sensors, derived from the distribution in absence of maltose.

populations, along with their relative contributions; the corresponding average macroscopic response is shown in Figure 5C.

Finally, we should note that in reality even the distribution measured for a sample with 20 mM maltose (high above the binding constant) does not correspond to homogeneous Cy3 quenching. Data shown in Figures 6A,B clearly indicate that the distribution measured at 20 mM maltose is still significantly broader than the expected response deduced from the free sensor distribution. This may reflect inherent heterogeneity in the protein acceptor response to maltose, originating in either the acceptor dye response or the protein conformation changes.

Discussion

Our results confirm the suitability of metal-affinity-mediated QD–protein self-assembly for use in single particle measurements, where control over the protein orientation on the QD and high affinity can be achieved.[20,21,29] This self-assembly process yields a heterogeneous distribution in the number of proteins (and acceptors) per QD conjugate, a feature shared by alternative functionalization methods such as the conjugation of biotinylated macromolecules to streptavidin-coated QDs or the direct coupling of antibodies onto carboxylic acid–QDs by EDC (ethyl(dimethylaminopropyl) carbodiimide) reaction chemistry. Control over the QD–biomolecule valence distribution is essential for QD-based sensor characterization. Our results indicate that metal-affinity-mediated conjugation yields the expected Poisson distribution for all average ratios and can therefore be accounted for in subsequent data analyses. In particular, the fraction of unconjugated QDs becomes less than

2% when $N \geq 4$ proteins per QD (Figure 3), as predicted from the Poisson statistics. In contrast, using commercial Streptavidin-coated QDs the spFRET study described in ref 25 showed that a significant fraction ($\sim$50%) of the QD–DNA conjugates were not engaged in FRET when mixed with $N = 12$ target acceptors, which may reflect heterogeneity in the QD functionalization, acceptor conjugation, or QD-to-single acceptor FRET efficiency.[24]

It should be noted that even though this heterogeneity exists, an approximate analysis of ensemble FRET measurements can still be performed assuming a homogeneous population using the relation:

$$\sum_{n=0}^{Nsat} p(N,n)\, E(n) \approx E(n = N) \qquad (5)$$

where *Nsat* corresponds to the maximum saturation number of dye-labeled proteins around a single QD. The error incurred using this approximation (i.e., deviation between the two models) strongly depends on the ratio r/R_0 and the average conjugate valence N; it becomes sizable for small values of N and r/R_0. When used to derive estimates for the separation distance for a particular donor–acceptor pair, this approximation usually yields an error in r values that decreases with increasing separation distance and vice versa; it is less than 10% for $r > R_0$. This condition is met for most QD–dye pairs, largely due to the finite QD size and Förster radius range $R_0 \approx 50-70$ Å. Overall, when $r < R_0$, the exact expression of the average FRET efficiency taking into account the distribution in conjugate valence should be employed to derive accurate information on any QD–bioreceptor–dye complexes (eqs 1 and 3).

Several sources contribute to the broadening of subpopulation histograms ($n = 0, 1 ...$). One source of experimental noise is due to photon shot noise arising from the discrete nature of photons detected by the photodiodes. Here, we evaluate the emission ratio distribution width caused by the photon shot noise as $\Delta\eta = \sqrt{\bar{\eta}(1-\bar{\eta})/T}$, where $\bar{\eta}$ is the average emission ratio and T is the threshold used for the selection of the fluorescence bursts.[1] For example, a threshold of 40 counts yields a maximum $\Delta\eta$ of 0.08. Another source of broadening in FRET efficiency distribution is the heterogeneity of the QDs' emission wavelengths: individual QDs in the same population possess narrow, distinct emission spectra which result in heterogeneous spectral overlaps with the acceptor absorption spectrum. As a consequence, even though the ensemble population exhibits a narrow PL emission spectrum, two distinct QDs of the same population may undergo different FRET efficiencies.[35] This effect can be minimized by selecting a QD population emitting in a rather flat region of the acceptor absorption spectrum, like the 540 nm QDs/RR pair used in this study. Finally, fluctuations in donor–acceptor separation distances and quantum yield may also participate in the subpopulation heterogeneity.

A promising application of single QD FRET techniques is the ultrasensitive biomolecular detection of binding events or bioreceptor conformational changes in response to interactions with a target. While ideally detection of one single particle could be sufficient to reveal the target presence, in practice unambiguous detection requires a minimal fraction of QDs engaged in

(35) Pons, T.; Medintz, I. L.; Sykora, M.; Mattoussi, H. *Phys. Rev. B* **2006**, *73*, 245302.

FRET interactions. This is due to the fact that histograms for the Poisson subpopulations overlap considerably (e.g., histograms for $n = 0$ and $n = 1$ in Figure 4) due to experimental noise and conjugate heterogeneity. As a result, a small fraction of QDs engaged in FRET may not be distinguished from the majority of unconjugated QDs. In this regard, direct conjugation of biomolecules to QDs providing a short donor–acceptor distance (thus high energy transfer efficiency) and good acceptor reemission are desirable. These conditions allow the donor–single acceptor ($n = 1$) distribution to be well separated from the dye–free donor ($n = 0$) distribution and thus yield higher detection sensitivity. This is particularly exemplified by comparing histograms for QD/dye pairs with high and low FRET efficiencies, as shown in Figure 4B, C.

These considerations are also valid for other sensing schemes similar to the maltose sensor studied in this work. Here target detection relies on the emission ratio changes upon target binding to the QD–receptor conjugate. The sensitivity is then strongly dependent on the amplitude of these changes and on the target–receptor binding constant.

Conclusion

We have shown that luminescent QDs are particularly suitable as energy donors for single particle FRET sensing, since they offer bright, stable, and spectrally narrow emissions along with limited acceptor direct excitation. In particular, we demonstrated that spFRET provides information about heterogeneity in population composition. It allowed characterization of individual QD bioconjugate structures and revealed that there is a distribution in the number of biomolecules per QD in a macroscopically homogeneous sample, an important parameter in sensor development based on QDs and FRET. In addition, our results demonstrated that solution phase spFRET detection using QDs offers complementary information to those collected from ensemble measurements. When applied to the detection of the sugar maltose spFRET provides additional insights into the simultaneous presence of several sensor subpopulations in the sample, representing for example QD–MBP conjugates bound to maltose mixed with unbound conjugates. Finally, our results confirm that spFRET and ensemble measurements provide similar information about average FRET efficiencies and donor–acceptor distances in self-assembled QD–protein bioconjugates.

As progress in designing and implementing new QD bioconjugation techniques will allow the development of specific QD-based biomolecular probes, QDs are expected to find increasing applications in a wide range of biological and biophysical studies. Intracellular sensing of protein interactions, ligand–receptor binding, and protein trafficking inside live cells and across the cell membranes will certainly benefit from our results and from the development of spFRET using QD donors in general.

Supporting Information Available: Absorption and emission spectra of the QDs and fluorophores; emission ratio distributions fitted to the Poisson distribution model for 540 nm QD–MBP95C–RR conjugates; schematics of the reagentless maltose sensor. This material is available free of charge via the Internet at http://pubs.acs.org.

JA0657253